Solute concentration at a well in non-Gaussian aquifers under constant and time-varying pumping schedule

Arianna Libera [a,*], Felipe P. J. de Barros [a,1], Monica Riva [b,c,2], Alberto Guadagnini [b,c,3]

[a] *Sonny Astani Department of Civil and Environmental Engineering, University of Southern California, Kaprielian Hall, 3620 S. Vermont Avenue, Los Angeles, CA 90089, USA*

[b] *Dipartimento di Ingegneria Civile e Ambientale, Politecnico di Milano, Piazza L. Da Vinci 32, 20133 Milano, Italy*

[c] *Department of Hydrology and Atmospheric Sciences, University of Arizona, Tucson, AZ 85721, USA*

* *Tel.: +1 213 740 0603*

E-mail address: libera@usc.edu

[1] *Corresponding author. Tel.: +1 213 740 6130*

E-mail address: fbarros@usc.edu

[2] *Tel.: +39 02 2399 6214*

E-mail address: monica.riva@polimi.it

[3] *Tel.: +39 02 2399 6263*

E-mail address: alberto.guadagnini@polimi.it

Abstract

Our study is keyed to the analysis of the interplay between engineering factors (i.e., transient pumping rates versus less realistic but commonly analyzed uniform extraction rates) and the heterogeneous structure of the aquifer (as expressed by the probability distribution characterizing transmissivity) on contaminant transport. We explore the joint influence of diverse (*a*) groundwater pumping schedules (constant and variable in time) and (*b*) representations of the stochastic heterogeneous transmissivity (T) field on temporal histories of solute concentrations observed at an extraction well. The stochastic nature of T is rendered by modeling its natural logarithm, $Y = \ln T$, through a typical Gaussian representation and the recently introduced Generalized sub-Gaussian (GSG) model. The latter has the unique property to embed scale-dependent non-Gaussian features of the main statistics of Y and its (spatial) increments, which have been documented in a variety of studies. We rely on numerical Monte Carlo simulations and compute the temporal evolution at the well of low order moments of the solute concentration (C), as well as statistics of the peak concentration (C_p), identified as the environmental performance metric of interest in this study. We show that the pumping schedule strongly affects the pattern of the temporal evolution of the first two statistical moments of C, regardless the nature (Gaussian or non-Gaussian) of the underlying Y field, whereas the latter quantitatively influences their magnitude. Our results show that uncertainty associated with C and C_p estimates is larger when operating under a transient extraction scheme than under the action of a uniform withdrawal schedule. The probability density function (PDF) of C_p displays a long positive tail in the presence of time-varying pumping schedule. All these aspects are magnified in the presence of non-Gaussian Y fields. Additionally, the PDF of C_p displays a bimodal shape for all types of pumping schemes analyzed, independent of the type of heterogeneity considered.

Abstract

Our study is keyed to the analysis of the interplay between engineering factors (i.e., transient pumping rates versus less realistic but commonly analyzed uniform extraction rates) and the heterogeneous structure of the aquifer (as expressed by the probability distribution characterizing transmissivity) on contaminant transport. We explore the joint influence of diverse (a) groundwater pumping schedules (constant and variable in time) and (b) representations of the stochastic heterogeneous transmissivity (T) field on temporal histories of solute concentrations observed at an extraction well. The stochastic nature of T is rendered by modeling its natural logarithm, $Y = \ln T$, through a typical Gaussian representation and the recently introduced Generalized sub-Gaussian (GSG) model. The latter has the unique property to embed scale-dependent non-Gaussian features of the main statistics of Y and its (spatial) increments, which have been documented in a variety of studies. We rely on numerical Monte Carlo simulations and compute the temporal evolution at the well of low order moments of the solute concentration (C), as well as statistics of the peak concentration (C_p), identified as the environmental performance metric of interest in this study. We show that the pumping schedule strongly affects the pattern of the temporal evolution of the first two statistical moments of C, regardless the nature (Gaussian or non-Gaussian) of the underlying Y field, whereas the latter quantitatively influences their magnitude. Our results show that uncertainty associated with C and C_p estimates is larger when operating under a transient extraction scheme than under the action of a uniform withdrawal schedule. The probability density function (PDF) of C_p displays a long positive tail in the presence of time-varying pumping schedule. All these aspects are magnified in the presence of non-Gaussian Y fields. Additionally, the PDF of C_p displays a bimodal shape for all types of pumping schemes analyzed, independent of the type of heterogeneity considered.

1. Introduction

Probabilistic characterizations of subsurface contaminant transport within well fields under practical operational conditions are cornerstones of modern groundwater management and risk analysis best practices. Modeling set-up and results rely on an appropriate assessment of multiple factors, including the spatial variability of hydrogeological variables and the adopted engineering controls (e.g., groundwater pumping and/or injection operations). In this study, we aim at exploring the feedback between transient versus uniform pumping schedules and Gaussian or non-Gaussian nature of the heterogeneous transmissivity (*T*) field in influencing contaminant concentration and its uncertainty at extraction wells. Therefore, our work analyzes the combined effects of (*a*) structural heterogeneity of properties characterizing geological media and (*b*) planned sequences of pumping cycles on solute concentrations recovered at pumping wells, including an appraisal of the corresponding uncertainties.

A sequence of predefined pumping intervals is typically scheduled by water management agencies to achieve a trade-off between maximization of the benefits to anthropogenic activities and minimization of the environmental footprint of the groundwater withdrawal process. Nonetheless, most studies focusing on probabilistic analyses of subsurface contaminant transport within well fields are limited to scenarios associated with constant extraction practices. For example, a number of studies (e.g., *Varljen and Shafer*, 1991; *Franzetti and Guadagnini*, 1996; *Cole and Silliman*, 1997; *Vassolo et al*., 1998; *Guadagnini and Franzetti*, 1999; *Riva et al.*, 1999; *van Leeuwen et al.*, 2000; *Feyen et al.*, 2001) employ numerical Monte Carlo simulations to quantify the uncertainty in the extension of well protection areas within randomly heterogeneous aquifers, under steady-state background groundwater flow and in the presence of a single or multiple wells operating at a constant rate. Additional examples of studies that consider the way solute transport is driven by one or more wells pumping at a constant extraction/injection rate include *Indelman and Dagan* (1999), *Riva et al.* (2006), *Siirila and Maxwell* (2012), *de Barros et al.* (2013b), *Pedretti and Fiori* (2013), *Pedretti et al.* (2013; 2014).

Despite its importance, the impact of transient pumping on solute transport has received much less attention (e.g., *Chang et al.*, 1992; *Vesselinov*, 2007; *Chen et al.*, 2012; *Leray et al.*, 2014). *Libera et al.* (2017) systematically investigate the effects of scheduling of pumping operations (i.e., considering transient vs. constant in time pumping) on contaminant solute breakthrough curves (BTCs) detected at the pumping well in a spatially heterogeneous multi-Gaussian log-conductivity field. These authors show that a transient pumping strategy can markedly affect the temporal pattern of BTCs. The results of this study elucidate the importance of the pumping sequence on uncertainty quantification of solute transport, risk analysis and contaminated site management. Transient flow effects on the delineation of wellhead protection areas (WHPA) or capture zones have been considered in a series of works. For instance, *Ramanarayanan et al.* (1995) highlight the importance of considering seasonal variations in pumping operations for WHPA delineation. *Reilly and Pullock* (1996) observe that transient flow conditions should be considered to properly characterize transport of solutes released near the boundary of the well. *Festger and Walter* (2002) and *Jacobson et al.* (2002) evaluate the effects on capture zones of temporal variations in the direction of the hydraulic gradient. *Jacobson et al.* (2002) illustrate how the uncertainty in the magnitude and direction of the mean regional flow influences the extent of time-dependent capture zones. *Neupauer et al.* (2014) study chaotic advection of a solute in an aquifer where a transient flow field is induced by injection and extraction sequences (see also *Piscopo et al.*, 2016).

In addition to pumping activities, the ubiquitous heterogeneity of hydraulic conductivity, K, or transmissivity T, is known to affect solute transport (e.g., *Dagan and Neuman,* 1997). High costs associated with site characterization contribute to hamper exhaustive reproductions of K-fields. This contributes to uncertainty associated with the quantitative description of transport scenarios. A common procedure adopted in stochastic hydrogeology is to assume a multivariate Gaussian distribution for the spatial field of log-conductivity, $Y = \ln K$. Spatial variability of hydrogeological attributes is, however, known to be more complex than described by a Gaussian model (e.g., *Gómez-Hernández and Wen,* 1998; *Wen and Gómez-Hernández,* 1998; *Willman et al.* 2008; *Fu and Gómez-Hernández,* 2009; *Mariethoz et al.*, 2010; *Haslauer et al.*, 2012; *Hu et al.*, 2013; *Xu and Gómez-Hernández,* 2015). In this context, high-resolution data analysis performed at the Macrodispersion Experiment (MADE) site, at the Columbus Air Force Base (Mississippi, USA), indicate that highly heterogeneous aquifers could be characterized in terms of non-Gaussian Y fields (*Meerschaert et al.*, 2013). *Fogg et al.* (1998) study alluvial heterogeneity in the Livermore Valley (California, USA) and question the ability of the multi-Gaussian assumption for Y to render an adequate description of the investigated area. *Rubin and Journel* (1991) point out that multi-Gaussian models can potentially fail in representing connected paths of extreme permeability values which might take place in the subsurface. This is also observed in other studies (e.g., *Journel and Deutsch*, 1993; *Sánchez-Vila et al.*, 1996; *Renard and Allard*, 2013) and the influence of such features on contaminant transport, risk assessment and groundwater remediation strategies has been highlighted in several works (e.g., *Silliman and Wright*, 1988; *Journel and Alabert*, 1989; *de Barros et al.*, 2013a; *de Barros et al.*, 2016 and references therein). Methods to generate synthetic random fields that reflect aspects of hydrogeologic structure and/or architecture, some of which may render such fields non-Gaussian, have been proposed (e.g., *Falivene et al.* 2006 and references therein).

A critical element which is emerging from a variety of studies is that the assumption of Gaussianity for Y is not consistent with features displayed by the sample probability distribution (and main statistical moments) of increments $\Delta Y(\boldsymbol{s}) = Y(\boldsymbol{x}) - Y(\boldsymbol{y})$ between two vector locations $\boldsymbol{x}$ and $\boldsymbol{y}$ ($\boldsymbol{s} = \boldsymbol{x} - \boldsymbol{y}$, denoting separation scale or lag). A common manifestation of this phenomenon is that while frequency distributions of Y often exhibit mild peaks and light tails, those of increments $\Delta Y(\boldsymbol{s})$ are typically symmetric with peaks that grow sharper, and tails that become heavier, as $s = \|\boldsymbol{s}\|$ decreases (e.g., *Liu and Molz*, 1997; *Painter*, 1996; *Meerschaert et al.*, 2004; *Riva et al.*, 2013a,b). Hydrogeologic variables that have been shown to exhibit such behaviors include log-permeabilities of porous and fractured geologic media (*Painter*, 1996; *Liu and Molz*, 1997; *Siena et al*., 2012; *Riva et al*., 2013a,b), neutron porosities in deep boreholes (*Guadagnini et al*., 2015), and soil composition data and hydraulic parameter estimates (*Guadagnini et al*., 2013, 2014) in a deep vadose zone. Manifestations of similar statistical scaling of a variety of Earth, environmental, ecological, biological, physical, astrophysical, and financial variables are reported, among others, by *Neuman et al*. (2013). As stated above, these features are clearly non compatible with a description of Y which is based on a Gaussian distribution model. *Painter* (1996) proposes to adopt Lévy-stable distributions to characterize permeability heterogeneity. *Strebelle* (2002) proposes an algorithm that utilizes multiple-point statistics inferred from training images to model conductivity fields. *Linde et al.* (2015) tackle the same problem through the use of training images based on hydrogeological facies mapping of nearby outcrops. *Haslauer et al.* (2012) employ non-Gaussian copula-based K models to study solute macrodispersion. A statistical framework that captures the disparate, scale-dependent distributions of Y and ΔY in a unified and consistent manner is offered by relying on the Generalized sub-Gaussian (GSG) model introduced by *Riva et al.* (2015a,b). In this context, *Riva et al.* (2017) explore analytically lead-order effects that non-Gaussian heterogeneity described by the GSG model has on the stochastic description of flow and transport under mean uniform steady-state flow in an unbounded, two-dimensional domain.

In light of the above, it is relevant to ask the following question: what is the feedback between transient pumping operations and the non-Gaussian nature of Y in influencing solute concentration and its uncertainty at the extraction well? Key research and operational questions driving our study are the following: how important are non-Gaussian conductivity features of the kind revealed when considering consistency between distributions of Y and its increments in transport when pumping is in operation? Does the pumping scheme overshadow the significance of non-Gaussian Y fields on statistics of solute concentration? Through a suite of computational studies, this work also enables to analyze the relative impact of the conductivity structure (i.e., Gaussian vs. non-Gaussian) on the solute concentration observed at the operating well in the presence of constant and time-varying pumping rates.

2. Problem Formulation

We consider a fully saturated two-dimensional (2D) confined porous formation identified by a Cartesian coordinate system, with vector location indicated by $\boldsymbol{x} = (x, y)$. A uniform-in-the-mean base flow q_0 takes place along the x-direction, and the transmissivity field, T, is spatially heterogeneous. The porous formation porosity and storativity, respectively denoted as φ and S, are considered to be constant. A pumping well is operating with an extraction rate $Q_w(t)$, with t

indicating time, at location $\boldsymbol{x_w} = (x_w, y_w)$. Figure 1 illustrates a sketch of the setting analyzed. Flow within the hydrogeological system is governed by:

$$S\frac{\partial h(\boldsymbol{x},t)}{\partial t} = \nabla \cdot [T(\boldsymbol{x})\nabla h(\boldsymbol{x},t)] + Q_w(t)\delta(\boldsymbol{x} - \boldsymbol{x}_w), \qquad (1)$$

where h denotes hydraulic head and δ represents the Dirac delta function. West (left) and east (right) boundaries of the porous formation (see Figure 1) are characterized by fixed hydraulic head values and no-flow boundary conditions are prescribed on the north and south boundaries of the domain.

A hazardous non-reactive solute is instantaneously released at time t_0 within an area A_0 (see Figure 1) with constant concentration c_0. The spatio-temporal evolution of the solute plume is assumed to be governed by the advection-dispersion equation:

$$\frac{\partial C(\boldsymbol{x},t)}{\partial t} - \nabla \cdot [\boldsymbol{D}\nabla C(\boldsymbol{x},t) - \boldsymbol{v}(\boldsymbol{x},t)C(\boldsymbol{x},t)] = 0$$
$$C(\boldsymbol{x},t_0) = c_0 \text{ for } \boldsymbol{x} \in A_0, \qquad (2)$$

where C indicates solute concentration and $\boldsymbol{v}$ is the Darcy-scale velocity (i.e., $\boldsymbol{v} = \boldsymbol{q}/\varphi$, $\boldsymbol{q}$ indicating specific discharge). Local-scale dispersion is given by the tensor $\boldsymbol{D}$, with components D_x and D_y, respectively along the *x* and *y*-direction (Figure 1). Note that Q_w in (1) is negative if extraction occurs and positive in case of injection. In our analysis, the prescribed head and flow boundary conditions are located sufficiently far away from the solute transport area to avoid boundary effects (*Rubin and Dagan*, 1989).

In the following, we investigate the way concentration breakthrough curves (BTCs) are affected by constant and transient pumping conditions. This analysis is carried out for Gaussian and/or non-Gaussian spatially random log-transmissivity fields as described in Section 3.

3. Methodology

3.1 Domain configuration and numerical implementation

We solve (1) and (2) within a 2D system of size of $\Omega = L_{sx} \times L_{sy}$, where $L_{sx} = 170\ m$, $L_{sy} = 150\ m$ (see Figure 1). Values of the main parameters adopted in this study are listed in Table 1. The values listed in Table 1 were selected for the purpose of illustration, all computational results being presented in dimensionless form. In agreement with the main results of previous works (*Leube et al.*, 2013; *Moslehi et al.*, 2015), the domain is discretized by a uniform grid formed of square elements of size $\Delta x = \Delta y = 1/8\ I$, with I being the characteristic integral scale of the random log-transmissivity, $Y = \ln T$, field. Details of the models adopted to describe the random nature of Y are provided in Section 3.2. The solute is instantaneously released over an aerial source zone A_0 of size $L_{sx} \times L_{sy}$ (see Figure 1). The barycenter of A_0 is located at distance L (measured along the *x*-direction) from an operating pumping well.

Following the work of *Libera et al.* (2017), which was based on an analysis of pumping strategies employed by groundwater management to satisfy diverse societal needs (e.g., drinking and irrigation), we adopt the pumping operation shown in Figure 2. A constant in time extraction strategy, here denoted by S_I, is depicted in Figure 2a. Figure 2b depicts the pattern of a withdrawal strategy that varies in time according to a predefined sequence, indicated by S_{II}. Note that, as explained in Section 1, most available studies refer to constant in time pumping scenarios that may not accurately represent realistic operations. The selected strategies (i.e., S_I and S_{II}) are characterized by the extraction of the same volume of groundwater across the simulation time.

For a given Y field, we employ the well-tested codes MODFLOW (*Harbaugh*, 2005) and MT3DMS (*Zheng and Wang*, 1999), respectively to solve the transient groundwater flow equation (1) and the advection-dispersion equation (2). Note that the groundwater flow equation (1) and the numerical model (i.e., MODFLOW) adopted do not consider possible additional effects (e.g., non-Darcian flow, skin effects, or storage) at the well. Solute transport is computed through the Method of Characteristics. To quantify uncertainty in the concentration C at the well, we employ a numerical Monte Carlo (MC) framework. Our analysis is based on a set of 10,000 MC simulations for each of the investigated scenarios. The choice of the size of the MC sample is based on a statistical convergence analysis (details not shown).

3.2 Random Y Model

As mentioned in Section 1, a variety of works emphasize the importance of adopting non-Gaussian Y fields in solute transport studies. In our analysis, we employ the GSG model introduced by *Riva et al.* (2015a,b) to generate multiple realizations of Y. As stated in the Introduction, this model has the key ability to embed in a unique theoretical framework the scale-dependent non-Gaussian features of the main statistics of Y and its increments taken at diverse lags, which have been documented in a variety of studies. The GSG model is here only briefly summarized for the sake of completeness, additional details being provided by *Riva et al.* (2015a,b).

We write zero-mean random fluctuations, $Y'(\boldsymbol{x}) = Y(\boldsymbol{x}) - \langle Y \rangle$, as

$$Y'(\boldsymbol{x}) = U(\boldsymbol{x})G(\boldsymbol{x}), \tag{3}$$

where $\langle \ \rangle$ denotes ensemble mean (expectation), $G(\boldsymbol{x})$ is a single- or multi-scale Gaussian random field and $U(\boldsymbol{x})$ is a non-negative subordinator independent of $G(\boldsymbol{x})$. The subordinator U consists of statistically independent identically distributed (iid) non-negative random values at all points $\boldsymbol{x}$. We consider the subordinator U to be log-normally distributed (other choices being possible) according to $U \equiv \mathcal{LN}[0, (2-\alpha)^2]$, where $\alpha < 2$. Note that in this case the PDF of Y' in

(3) coincides with the classical normal-lognormal model (see, e.g., *Guadagnini et al.*, 2015 and references therein).

To investigate the effects of Gaussian versus non-Gaussian Y fields on solute transport we consider two forms of Y: sub-Gaussian (see (3)), Y_{SG}, and Gaussian, Y_G. The latter is obtained from the former when $\alpha \to 2$. For the purpose of comparison, we consider these two forms of the Y field to have equal mean values, i.e. $\langle Y \rangle = \langle Y_{SG} \rangle = \langle Y_G \rangle = 0$, variances $\sigma_Y^2 = \sigma_{Y\,SG}^2 = \sigma_{Y\,G}^2$ and integral scales $I = I_{Y_{SG}} = I_{Y_G}$. The Gaussian random function, $G(\boldsymbol{x})$, in (3) constitutes a truncated fractional Brownian motion (tfBm) with truncated power variogram (*Di Federico and Neuman*, 1997):

$$\gamma_G^2(s) = \gamma^2(s; \lambda_u) - \gamma^2(s; \lambda_l), \tag{4}$$

where

$$\gamma^2(s, \lambda_m) = \frac{\mathcal{A}\lambda_m^{2H}}{2H}\left[1 - exp\left(-\frac{s}{\lambda_m}\right) + \left(\frac{s}{\lambda_m}\right)^{2H} \Gamma\left(1 - 2H, \frac{s}{\lambda_m}\right)\right], \quad m = l, u. \tag{5}$$

Quantities λ_u and λ_l in equations (4)-(5) are the lower and upper cutoff scales of the variogram model, respectively proportional to the length scales of data support and domain size; H is the Hurst coefficient and $\mathcal{A}$ is a constant. This choice of variogram model is consistent with documented scaling phenomena, including power-law scaling of sample structure functions (including the variogram of Y) in midranges of lags and nonlinear scaling of power-law exponent with order of sample structure function (e.g., *Guadagnini et al.*, 2012, 2013, 2014, 2015; *Panzeri et al.*, 2016; *Riva et al.*, 2013a, 2013b; *Siena et al.*, 2012; *Siena et al*. 2014). As such, equation (4) allows bridging across scales by analyzing jointly data characterized by diverse support/measurement scales across windows (observation domains) of diverse size at a site (*Neuman et al.*, 2008).

We simulate three diverse collections (ensembles) of non-Gaussian Y_{SG} fields (each constituted by 10,000 realizations) distinguished by three values of the parameter α (= 1.2, 1.5, 1.8, representing strong to relatively mild departure from a Gaussian behavior) and one set of Gaussian Y_G fields (also with 10,000 realizations). Input parameters used to generate Y_G and Y_{SG} fields are listed in Table 2 (input values employed to generate Y_G are listed in the column labeled $\alpha \rightarrow 2$). Each Gaussian and non-Gaussian collection/ensemble of log-transmissivity realizations is coupled with both pumping strategies adopted (S_I and S_{II}, see Figure 2) within the numerical MC framework. Therefore, we perform a total number of 80,000 MC simulations.

4. Results and discussion

This section is structured as follows: we start by presenting the temporal evolution of the low order statistics (mean and variance) of the contaminant concentration, C, recovered at an observation well placed, for simplicity, at the same location of the pumping well. Then, we focus on the analysis of the peak concentration, C_p, observed at the well. The latter represents an important quantity for the management and remediation of polluted areas and can be used as proxy for dilution (*Fiori,* 2001). All analyses are performed for the two pumping strategies, namely S_I (constant in time) and S_{II} (variable in time), illustrated in Figure 2. Diverse values of the parameter α are considered (see Section 3.2) for each pumping scenario. We present all results in dimensionless form. The concentration is normalized by C^*, which represents a contaminant concentration threshold, as established, for instance, by environmental protection agencies (e.g., EPA). Here we set, without loss of generality to our methodological approach, $C^* = 10\ g/m^3$. The selected value of the critical concentration is in line with the EPA's Maximum Contaminant Level (MCL) for nitrate (see *US EPA*, 2009), and is employed for the purpose of illustration in our study.

Time is normalized by I/v_0, with $v_0 = q_0/\varphi$, $q_0 = T_G J$ and $T_G = \exp(\langle Y \rangle)$. The pumping rate Q_w is normalized by Q_0, where $Q_0 = q_0 L_y$ represents the uniform-in-the-average water flow discharge. The longitudinal Péclet number, $P_e = I v_0/D_x$, is set to 800 (see Table 1). Parameter values employed in this synthetic analysis allow illustrating the interplay between pumping well operations and natural heterogeneity of the porous formation.

4.1 Temporal evolution of low-order moments of solute concentration at the well

Figure 3 depicts the temporal Monte Carlo based pattern of the dimensionless mean of the solute concentration, $\langle C \rangle / C^*$, observed at the well location. Results depicted in Figure 3a, b respectively refer to the pumping scheme S_I (constant withdrawal) and S_{II} (time-dependent withdrawal). Each mean concentration BTC presented in Figures 3a and 3b refers to a given value of α. Regardless the value of α, the mean concentration BTC displays a unimodal behavior under conditions associated with S_I and a multimodal pattern when the scheme S_{II} is active. The multimodal pattern observed in Figure 3b descends from the observation that a time-dependent pumping rate (S_{II}) induces temporal oscillations of the mean contaminant BTC. The impact of variable pumping rate on concentration statistics was analyzed by *Libera et al.* (2017) for Gaussian Y fields. Figure 3b suggests that solute dilution is induced during the time periods when pumping is active. Increased pumping rates would lead to an enlargement of the catchment region (e.g., *Bear*, 1979). Hence, an increased volume of clean water would be captured (on average) at the well together with the solute plume. Therefore, the mean concentration decreases within these intervals because of the mixing of polluted water with clean water. We also note that the largest values of $\langle C \rangle$ occur within the strongly non-Gaussian Y field characterized by $\alpha = 1.2$ for both scenarios S_I and S_{II}. As shown in Figure 3, the maximum value of $\langle C \rangle$ decreases as α increases towards 2, i.e. as the Y field tends to be Gaussian. We note that the differences in $\langle C \rangle$ between the

Gaussian case ($\alpha \rightarrow 2$) and the GSG setting characterized by $\alpha = 1.8$ are negligible. Based on the results of Figure 3, we conclude that the pumping regime (S_I or S_{II}) controls the pattern of the temporal evolution of the mean contaminant BTC, regardless of the value of α. The general shape of the temporal evolution of $\langle C \rangle$ is, in fact, very similar for all values of α considered, as observed in both Figures 3a and 3b.

Figures 4a and 4b depict the dimensionless variance of the solute concentration, $Var[C]/C^{*2}$, versus dimensionless time for all values of α analyzed, respectively for S_I and S_{II}. The pumping strategy clearly controls the general pattern of the temporal evolution of $Var[C]$, regardless the value of α, i.e., a unimodal pattern of $Var[C]$ is identified for constant pumping (Figure 4a) while a multimodal behavior of $Var[C]$ is induced by temporal variability in the pumping rate (Figure 4b). We note that $Var[C]$ in Figure 4b decreases when pumping is active, indicating that the variability across the MC ensemble is smaller when the solute is attracted to the well by the start of pumping. In this situation, the likelihood that the solute plume is captured by the well increases and the variability of concentration values at the well decreases. We then observe that $Var[C]$ increases approximately by an order of magnitude under regime S_{II} (compare Figure 4b and Figure 4a), these results being in line with the conclusions of *Libera et al.* (2017). On these bases, one can see that the choice of the pumping extraction operation (e.g., constant in time S_I, as considered in most literature works, versus transient S_{II}, which is more realistic) has a key role on quantification of the uncertainty associated with the concentration at the well. Amongst other factors, this is also related to the observation that a constant pumping scheme always controls the same portion of the flow field at all times. Otherwise, a transient pumping schedule enables to extend the influence of the well to diverse portions of the heterogeneous system, depending on time. As such, the effect of the aquifer heterogeneous structure plays an enhanced role under pumping scenario S_{II} than in the presence of S_I, resulting in an overall increase of $Var[C]$ at the well. We then observe that the increase of the concentration variance is magnified for the lowest values of α, i.e., as the departure of the GSG fields from Gaussianity increases. We remark that the differences in $Var[C]$ between the Gaussian case ($\alpha \rightarrow 2$) and the setting characterized by $\alpha = 1.8$ are negligible, similar to what we observed for $\langle C \rangle$.

In summary, the analysis of Figures 3 and 4 lead to the conclusion that the pumping scheme selection (S_I or S_{II}) clearly influences the temporal pattern (unimodal or multimodal) of the pollutant BTCs lead-order statistics (as expressed by mean and variance). The actual magnitude of the first and second moment of C is controlled by both the pumping scheme and the structural representation (Gaussian or non-Gaussian) of Y.

4.2 Statistical analysis of the peak concentration

Here we analyze key statistical features of the peak value of the solute concentration, C_p, observed at the well. This quantity is an important environmental performance metric (EPM) for risk analysis (*de Barros et al.*, 2012) and, as previously stated, can also be used as a proxy for dilution (*Fiori*, 2001).

4.2.1 Outliers in the peak concentration distribution

We present the box plots of C_p in Figure 5 for pumping operational setting S_I and for the diverse values of α analyzed. Figure 6 depicts corresponding results for scenario S_{II}. We recall that the thickness of the box plots corresponds to the lag between the first and third quartiles of the probability distribution. Close inspection of Figures 5 and 6 evidences a considerable number of outside values (or outliers), identified in red and corresponding to the observations that fall outside the whiskers (represented by horizontal segments connected through dashed lines to the boxplots of Figures 5 and 6) under the action of both extraction schemes. Note that the upper whisker corresponds to the largest value observed given that the length of the dashed lines is 1.5 times the interquartile range, the same criteria applies to the lower whisker. Comparing Figures 5 and 6 suggests that the range of C_p values is broadest when S_{II} is active. In this case the largest values of normalized C_p are roughly three times larger than the corresponding extreme values of C_p computed under scheme S_I. We also note that the number of such high values generally tends to decrease as the nature of the underlying log-transmissivity field tends to Gaussian (i.e., increasing α) for both pumping scenarios. This evidence suggests that the nature of the heterogeneous structure of Y influences the distribution of C_p. These observations are consistent with the fact that a non-Gaussian Y structure increases the likelihood of the occurrence of well-connected zones of low and high conductivity (as manifested through high peaks of increment PDFs at short lags, whose effects are increasingly pronounced with departure from the Gaussian behavior). This specific feature is allowed to emerge in a stronger way in the presence of transient pumping than for constant extraction as already noticed in section 4.1 for the mean and variance of C.

4.2.2 Probability density function of the maximum concentration

Figure 7 depicts the sample PDF, $p(C_p)$, of the peak concentration detected at the well for pumping scenario S_I and all values of α investigated. For completeness, the sample cumulative distribution function (CDF) of C_p, $P(C_p)$, is also depicted. Corresponding plots for scenario S_{II} are included in Figure 8. The action of the transient pumping regime S_{II} contributes to distribute the observed values of C_p across a wider range than that documented for S_I (compare Figures 7 and 8). As such, the PDF of C_p for S_{II} generally encompasses a broader range of values and is characterized by longer positive tails than the PDF of C_p resulting from S_I. These observations are consistent with the results depicted in the inset plots of Figures 5 and 6. The positive tails of the PDFs are quantitatively affected by the parameter α. Non-Gaussian Y fields are characterized by an increased probability of observing higher C_p at the well, when compared to Gaussian Y fields ($\alpha \to 2$), thus yielding enhanced tailing for $p(C_p)$. This behavior is consistent with our earlier observations according to which the GSG nature of the Y field leads to an increased likelihood that solute can be conveyed through connected paths of high conductivity, thus yielding an increased tailing in the PDFs of C_p (i.e., higher C_p values). Similar to what observed in Section 4.1, results for the Gaussian Y field virtually coincide with those obtained for $\alpha = 1.8$. This result further emphasizes the challenges of distinguishing between these types of fields (for relatively large values of α) solely on the basis of system responses (e.g., in this cases, concentrations detected at the well).

One can note a bimodal shape for $p(C_p)$ in both Figures 7 and 8. This feature can be attributed to the observation that very low or no concentration signals are observed at the pumping well (i.e., the solute plume does not hit the well) across some MC realizations, a significant portion of the plume being captured in other MC realizations (e.g., *Bellin and Tonina*, 2007). Note that while the observation that $p(C_p)$ tends to be bimodal in the presence of pumping wells is a significant result, this bimodal pattern in the PDF can change in the presence of other factors, including, e.g., increased travel distance between contaminant source and operating well and change of Péclet number. While of definite interest, these analyses are outside the scope of our current contribution.

4.2.3 Average of the maximum concentration

We quantify here the impact of the pumping operation schedule and of the Y field structure on the average value of the peak concentration $\langle C_p \rangle$. We do so by computing the relative change of $\langle C_p \rangle$ obtained across the collection of Y_{SG} MC realizations with respect to the corresponding result associated with a Gaussian (Y_G) field as:

$$\eta = \left| \frac{\langle C_p(t;\alpha,S_i) \rangle - \langle C_p(t;\alpha \to 2,S_i) \rangle}{\langle C_p(t;\alpha \to 2,S_i) \rangle} \right|, \quad i = I, II \tag{6}$$

Figure 9 depicts η versus α for scenario S_I (light grey) and S_{II} (dark grey). These results suggest that $\langle C_p \rangle$ is more sensitive to the value of α when the spatially heterogeneous flow field is stressed according to scheme S_{II} than it does for S_I. As shown in Figure 9, the magnitude of η is larger for scenario S_{II} (dark grey) and decreases as α increases, i.e. transitioning from a GSG to a Gaussian Y field. The response of the system due to a Gaussian Y field ($\alpha \to 2$) is virtually indistinguishable from that associated with values of $\alpha \geq 1.8$.

5. Conclusions

This study investigates the impact of the model employed to describe the random spatial heterogeneity of the aquifer log-transmissivity field (Y) on the statistics of the solute concentration (C) at a pumping well in the presence of two distinct pumping regimes. We consider a Gaussian and a Generalized sub-Gaussian (GSG, see equation (3)) model to describe the randomly heterogeneous Y field. In the following, we briefly summarize the key conclusions emerged from the analysis.

The pumping scheme influences the shape of the temporal evolution of mean, $\langle C \rangle$, and variance, $Var[C]$, of C whereas the choice of the Y structural representation, as quantified by the value of α in this study, controls their magnitude. Transient pumping produces a multimodal behavior (whereas constant pumping results in a unimodal pattern) of $\langle C \rangle$ and $Var[C]$. The multimodal behavior of $\langle C \rangle$ is characterized by its lowest values taking place during stress periods of water pumping, the decrease in $\langle C \rangle$ being due to contaminant dilution with fresh water. We also observe that $Var[C]$ tends to decrease during pumping time intervals. This behavior is related to the effect of the well operation which increases the likelihood that the plume is captured by attracting water and hence results in a decreased variability of C at the well. Values of $Var[C]$ are roughly one order of magnitude larger under transient pumping than in the presence of constant extraction. As such, engineering control (as manifested through selected pumping schedules) plays a marked role in the uncertainty associated with C.

The highest values of solute peak concentration, C_p, are prone to be observed at a well operating according to a time-varying schedule. This feature is amplified in the presence of values of α associated with an increased departure of the GSG Y field from a Gaussian behavior. The PDF of C_p, $p(C_p)$, is characterized by a bimodal shape for all cases analyzed in this study.

Our analysis shows that statistical moments (and PDFs) of C and C_p obtained within a GSG Y field identified by relatively large α values, i.e. $\alpha = 1.8$, and a Gaussian Y field are virtually indistinguishable. This result is consistent with the recent findings of *Riva et al*. (2017). These authors explore analytically lead-order effects that non-Gaussian heterogeneity described by the GSG model have on the stochastic description of flow and transport under uniform in the mean flow in two-dimensional unbounded randomly heterogeneous media. Their results indicate that differences between lead-order flow and transport moments associated with GSG and Gaussian

Y fields tend to diminish as α approaches 2, becoming virtually unnoticeable for $\alpha \geq 1.8$. Similar to these authors, our results indicate the existence of a threshold value for α above which the effects associated with the non-Gaussian nature of the heterogeneous conductivity structure are virtually undetectable in the concentration BTCs recorded at the well. A value of $\alpha = 1.8$ can be considered as a threshold above which the impact of the Y distribution (i.e. Gaussian vs non-Gaussian) is shadowed when compared to the influence of the engineering control (i.e., groundwater pumping rate) selected. Note that while these results appear to indicate that commonly employed Gaussian models could reproduce key transport features even in the presence of non-Gaussian Y fields, they also suggest that it would be difficult to differentiate between Gaussian and non-Gaussian Y fields on the basis of such moments when α is close but not equal to 2. Such a distinction can be validly drawn only by analyzing Y data and their increments jointly, as suggested by *Riva et al.* (2015a).

The outcomes of our work associated with the feedback between engineering factors (i.e., transient versus uniform pumping rates) and efforts aimed at the characterization of aquifer heterogeneous structure (through Gaussian or Sub-Gaussian models) on the behavior of contaminant BTCs are of potential interest to direct technical and economical efforts towards an optimal management of groundwater resources. For example, costs linked to an increase of the well pumping rate could be justified by the production of water characterized by low contaminant concentrations, which in turn leads to decreased water treatment costs. Our results also suggest that pumping operations can control the temporal patterns of risk and might overshadow the impact of the type of aquifer heterogeneity (as embedded in the functional format of the probability density function characterizing hydraulic conductivity) on BTCs at pumping wells. In this framework, there could be circumstances in which enhanced efforts should be allocated towards an improved optimal planning of the pumping regime as opposed to a detailed characterization of some features of the heterogeneous properties of an aquifer. Such allocation of resources is key to reduce the uncertainty in risk metrics and is well aligned with goal-oriented site characterization frameworks (*de Barros et al.*, 2012 and references therein). As a future research outlook, it would be of interest to extend our analysis to investigate transport in realistic systems of increased level of complexity that incorporate stochastic fluctuations for water demand.

Additionally, extending the findings of our work to three dimensional aquifers' configurations in the presence of pumping wells operating with transient rates is focus of future research. We believe that increasing the dimensionality of the system, i.e. from a 2D to a 3D configuration, would enable to capture more realistic flow paths that would potentially enhance solute mixing. As shown in *Dentz and de Barros* (2013), the uncertainty of the overall solute dispersive behavior and its self-averaging properties are affected by the dimensionality of the flow field. The dilution enhancement induced by the additional degree of freedom within a three-dimensional setting would yield a decrease of the solute concentration variability across Monte Carlo realizations with an ensuing decrease of the associated variance. Varying the dimensionality of the flow field (i.e., considering a three-dimensional system) might also affect the scaling behavior of the contaminant BTCs observed at the operating well (e.g., *Pedretti et al*., 2013, 2014) due to increased connectivity of the permeability field (*Di Dato et al.*, 2017).

Acknowledgments

The first author gratefully acknowledges the financial support provided by Foundation for Cross Connection Control and Hydraulic Research at the University of Southern California. Funding from the EU and MIUR (Italian Ministry of Education, University and Research) under the Water JPI, WaterWorks 2014 framework (project: WE-NEED-Water NEEDs, availability, quality and sustainability) is also acknowledged. The authors acknowledge the constructive comments raised by three anonymous reviewers.

References

Bear, J., 1979. Hydraulics of groundwater. McGraw-Hill, Inc., New York.

Bellin, A., Tonina, D., 2007. Probability density function of non-reactive solute concentration in heterogeneous porous formations. J. Contam. Hydrol. 94(1), 109-125.

Chang, L. C., Shoemaker, C. A., Liu, P. L. F., 1992. Optimal time-varying pumping rates for groundwater remediation: Application of a constrained optimal control algorithm. Water Resour. Res. 28 (12), 3157-3173.

Chen, Y., Lu, C., Luo, J., 2012. Solute transport in divergent radial flow with multistep pumping. Water Resour. Res. 48, W02510, doi:10.1029/2011WR010692.

Cole, B., Silliman, S., 1997. Capture zones for passive wells in heterogeneous unconfined aquifers. Ground Water 35 (1), 92-98.

Dagan, G., Neuman, S. P., 1997. Subsurface flow and transport: a stochastic approach. Cambridge University Press.

de Barros, F. P. J., Bellin, A., Cvetkovic, V., Dagan, G., Fiori, A., 2016. Aquifer heterogeneity controls on adverse human health effects and the concept of the hazard attenuation factor. Water Resour. Res. 52(8), 5911-5922.

de Barros, F. P. J., Ezzedine, S., Rubin, Y., 2012. Impact of hydrogeological data on measures of uncertainty, site characterization and environmental performance metrics. Adv. Water Resour. 36, 51-63.

de Barros, F. P. J., Fernàndez-Garcia, D., Bolster, D., Sanchez-Vila, X., 2013a. A risk-based probabilistic framework to estimate the endpoint of remediation: Concentration rebound by rate-limited mass transfer. Water Resour. Res. 49(4), 1929-1942.

de Barros, F. P. J., Guadagnini, A., Fernàndez-Garcia, D., Riva, M., Sanchez-Vila, X., 2013b. Controlling scaling metrics for improved characterization of well-head protection regions. J. Hydrol. 494, 107-115.

Dentz, M., de Barros F. P. J., 2013. Dispersion variance for transport in heterogeneous porous media. Water Resour. Res. 49(6): 3443–61. http://dx.doi.org/10. 1002/wrcr.20288.

Di Dato, M., Fiori, A., de Barros, F. P. J. and Bellin, A., 2017. Radial solute transport in highly heterogeneous aquifers: Modeling and experimental comparison. Water Resour. Res. In Press. doi:10.1002/2016WR020039.

Di Federico, V., Neuman, S. P., 1997. Scaling of random fields by means of truncated power variograms and associated spectra. Water Resour. Res. 33, 1075–1085.

Falivene, O., Arbués, P., Gardiner, A., Pickup, G., Muñoz, J. A., Cabrera, L, 2006. Best practice stochastic facies modeling from a channel-fill turbidite sandstone analog (the Quarry outcrop, Eocene Ainsa basin, northeast Spain). AAPG Bull. 90, 1003-1029.

Feyen, L., Beven, K. J., De Smedt, F., Freer, J., 2001. Stochastic capture zone delineation within the generalized likelihood uncertainty estimation methodology: conditioning on head observations. Water Resour. Res. 37 (3), 625-638.

Festger, A. D., Walter, G. R., 2002. The capture efficiency map: the capture zone under time-varying flow. Ground Water 40 (6), 619-628.

Fiori, A., 2001. The Lagrangian concentration approach for determining dilution in aquifer transport: Theoretical analysis and comparison with field experiments. Water Resour. Res. 37(12), 3105-3114.

Fogg, G. E., Noyes, C. D., Carle, S. F., 1998. Geologically based model of heterogeneous hydraulic conductivity in an alluvial setting. Hydrol. J. 6, 131–143.

Franzetti, S., Guadagnini, A., 1996. Probabilistic estimation of well catchments in heterogeneous aquifers. J. Hydrol. 174 (1), 149-171.

Fu, J., Gómez-Hernández, J. J., 2009. Uncertainty assessment and data worth in groundwater flow and mass transport modeling using a blocking Markov chain Monte Carlo method. J. Hydrol. 364(3), 328-341, doi: 10.1016/j.jhydrol.2008.11.014.

Gómez-Hernández, J. J., Wen, X. H., 1998. To be or not to be multi-Gaussian? A reflection on stochastic hydrogeology. Adv. Water Resour. 21(1), 47-61. doi:10.1016/S0309-1708(96)00031-0.

Guadagnini, A., Franzetti, S., 1999. Time-related capture zones for contaminants in randomly heterogeneous formations. Ground Water 37 (2), 253-260.

Guadagnini, A., Riva, M., Neuman, S. P., 2012. Extended power-law scaling of heavy-tailed random air-permeability fields in fractured and sedimentary rocks. Hydrol. Earth Syst. Sci. 16, 3249–3260, doi: 10.5194/hess-16-3249-2012.

Guadagnini, A., Neuman, S. P., Schaap, M. G., Riva, M., 2013. Anisotropic statistical scaling of vadose zone hydraulic property estimates near Maricopa, Arizona. Water Resour. Res. 49, doi:10.1002/2013WR014286.

Guadagnini, A., Neuman, S. P., Schaap, M. G., Riva, M., 2014. Anisotropic statistical scaling of soil and sediment texture in a stratified deep vadose zone near Maricopa, Arizona. Geoderma 214, 217-227, doi:10.1016/j.geoderma.2013.09.008.

Guadagnini, A., Neuman, S. P., Nan, T., Riva, M., Winter, C. L., 2015. Scalable statistics of correlated random variables and extremes applied to deep borehole porosities. Hydrol. Earth Syst. Sci. 19, 19, 1–17, doi:10.5194/hess-19-1-2015.

Harbaugh, A. W., 2005. MODFLOW-2005, the US Geological Survey modular groundwater model: the ground-water flow process. US Department of the Interior, US Geological Survey, Reston, VA, USA, pp. 6–A16.

Haslauer, C. P., Guthke, P., Bárdossy, A., Sudicky, E. A., 2012. Effects of non-Gaussian copula-based hydraulic conductivity fields on macrodispersion. Water Resour. Res. 48, W07507, doi:10.1029/2011WR011425.

Hu, L., Zhao, Y., Liu, Y., Scheepens, C., Bouchard, A., 2013. Updating multipoint simulations using the ensemble Kalman filter. Comput. Geosci. 51, 7-15, doi:10.1016/j.cageo.2012.08.020.

Indelman, P., Dagan, G., 1999. Solute transport in divergent radial flow through heterogeneous porous media. J. Fluid Mech. 384, 159-182.

Jacobson, E., Andricevic, R., Morrice, J., 2002. Probabilistic capture zone delineation based on an analytic solution. Ground Water 40 (1), 85-95.

Journel, A. G., Alabert, F. G., 1989. Non-gaussian data expansion in the Earth Sciences. Terra Nova 1, 123–134.

Journel, A. G., Deutsch, C. V., 1993. Entropy and spatial disorder. Math. Geol. 25(3), 329-355.

Leray, S., de Dreuzy, J. R., Aquilina, L., Vergnaud-Ayraud, V., Labasque, T., Bour, O., Le Borgne, T., 2014. Temporal evolution of age data under transient pumping conditions. J. Hydrol. 511, 555-566.

Leube, P. C., de Barros, F. P. J., Nowak, W., Rajagopal, R., 2013. Towards optimal allocation of computer resources: trade-offs between uncertainty quantification, discretization and model reduction. Environ. Model. Softw. 50, 97–107. http://dx. doi.org/10.1016/j.envsoft.2013.08.008.

Libera, A., de Barros, F. P. J., Guadagnini, A., 2017. Influence of pumping operational schedule on solute concentrations at a well in randomly heterogeneous aquifers. J. Hydrol. 546, 490-502.

Linde, N., Lochbühler, T., Dogan, M., Van Dam, R. L., 2015. Tomogram-based comparison of geostatistical models: Application to the Macrodispersion Experiment (MADE) site. J. Hydrol. 531, 543-556.

Liu, H. H., Molz, F. J., 1997. Comment on ‘‘Evidence for non-Gaussian scaling behavior in heterogeneous sedimentary formations’’ by Scott Painter. Water Resour. Res. 33(4), 907 – 908.

Mariethoz, G., Renard, P., Straubhaar, J., 2010. The direct sampling method to perform multiple-point geostatistical simulations. Water Resour. Res. 46, W11536, doi:10.1029/2008WR007621.

Meerschaert, M. M., Kozubowski, T. J., Molz, F. J., Lu, S., 2004. Fractional Laplace model for hydraulic conductivity. Geophys. Res. Lett. 31(8).

Meerschaert, M. M., Dogan, M., Dam, R. L., Hyndman, D. W., Benson, D. A., 2013. Hydraulic conductivity fields: Gaussian or not?. Water Resour. Res. 49(8), 4730-4737.

Moslehi, M., Rajagopal, R., de Barros, F. P. J., 2015. Optimal allocation of computational resources in hydrogeological models under uncertainty. Adv. Water Resour. 83, 299-309.

Neuman, S. P., Riva, M., Guadagnini, A., 2008. On the geostatistical characterization of hierarchical media. Water Resour. Res. 44, W02403, doi:10.1029/2007WR006228.

Neuman, S. P., Guadagnini, A., Riva, M., Siena, M., 2013. Recent advances in statistical and scaling analysis of earth and environmental variables. In: Mishra, P.K., Kuhlman, K.L. (Eds.). Advances in Hydrogeology. Springer Science+Business Media New York, 11-15, ISBN 978-1-4614-6478-5.

Neupauer, R. M., Meiss, J. D., Mays, D. C., 2014. Chaotic advection and reaction during engineered injection and extraction in heterogeneous porous media. Water Resour. Res. 50 (2), 1433-1447.

Painter, S., 1996. Evidence for non-Gaussian scaling behavior of heterogeneous sedimentary formations. Water Resour. Res. 32, 1183-1195.

Panzeri M., Riva, M., Guadagnini, A., Neuman, S. P., 2016. Theory and generation of conditional, scalable sub-Gaussian random fields. Water Resour. Res. 52, doi: 10.1002/2015WR018348.

Pedretti, D., Fiori, A., 2013. Travel time distributions under convergent radial flow in heterogeneous formations: Insight from the analytical solution of a stratified model. Adv. Water Resour. 60, 100-109.

Pedretti, D., Fernàndez-Garcia, D., Bolster, D., Sanchez-Vila, X., 2013. On the formation of breakthrough curves tailing during convergent flow tracer tests in three-dimensional heterogeneous aquifers. Water Resour. Res. 49(7), 4157-4173.

Pedretti, D., Fernàndez-Garcia, D., Sanchez-Vila, X., Bolster, D., Benson, D. A., 2014. Apparent directional mass-transfer capacity coefficients in three-dimensional anisotropic heterogeneous aquifers under radial convergent transport. Water Resour. Res. 50(2), 1205-1224.

Piscopo, A. N., Neupauer, R. M., Kasprzyk, J. R., 2016. Optimal design of active spreading systems to remediate sorbing groundwater contaminants in situ. J. Contam. Hydrol. 190, 29-43.

Ramanarayanan, T. S., Storm, D. E., Smolen, M. D., 1995. Seasonal pumping variation effects on wellhead protection area delineation. Water Resour. Bull. 31, No. 3: 421-430.

Reilly, T. E., Pollock, D. W., 1996. Sources of water to wells for transient cyclic systems. Ground Water 34 (6), 979-988.

Renard, P., Allard, D., 2013. Connectivity metrics for subsurface flow and transport. Adv. Water Resour. 51, 168-196.

Riva, M., Guadagnini, A., Ballio, F., 1999. Time-related capture zones for radial flow in two dimensional randomly heterogeneous media. Stoch. Env. Res. Risk A. 13 (3), 217-230.

Riva, M., Guadagnini, A., De Simoni, M., 2006. Assessment of uncertainty associated with the estimation of well catchments by moment equations. Adv. Water Resour. 29 (5), 676-691.

Riva, M., Neuman, S. P., Guadagnini, A., 2013a. Sub-Gaussian model of processes with heavy tailed distributions applied to permeabilities of fractured tuff. Stochastic Environ. Res. Risk Assess. 27, 195–207, doi: 10.1007/s00477-012-0576-y.

Riva, M., Neuman, S. P., Guadagnini, A., Siena, M., 2013b. Anisotropic scaling of Berea sandstone log air permeability statistics. Vadose Zone J. 12(3), 1–15, doi:10.2136/vzj2012.0153.

Riva, M., Neuman, S. P., Guadagnini, A., 2015a. New scaling model for variables and increments with heavy-tailed distributions. Water Resour. Res. 51, 4623-4634, doi:10.1002/2015WR016998.

Riva M., Panzeri, M., Guadagnini, A., Neuman, S. P., 2015b. Simulation and analysis of scalable non-Gaussian statistically anisotropic random functions. J. Hydrol. 531 Part 1, 88-95, doi:10.1016/j.jhydrol.2015.06.066.

Riva, M., Guadagnini, A., Neuman, S. P., 2017. Theoretical analysis of non-Gaussian heterogeneity effects on subsurface flow and transport. Water Resour. Res. 53, doi:10.1002/2016WR019353.

Rubin, Y., Journel, A. G., 1991. Simulation of non-Gaussian space random functions for modeling transport in groundwater. Water Resour. Res. 27.7, 1711-1721.

Rubin, Y., Dagan, G., 1989. Stochastic analysis of boundaries effects on head spatial variability in heterogeneous aquifers: 2. Impervious boundary. Water Resour. Res. 25(4), 707–712, doi:10.1029/WR025i004p00707.

Sánchez-Vila, X., Carrera, J., Girardi, J. P., 1996. Scale effects in transmissivity. J. Hydrol. 183(1-2), 1-22.

Siena, M., Guadagnini, A., Riva, M., Neuman, S. P., 2012. Extended power-law scaling of air permeabilities measured on a block of tuff. Hydrol. Earth Syst. Sci. 16, 29-42, doi:10.5194/hess-16-29-2012.

Siena, M., Guadagnini, A., Riva, M., Bijeljic, B., Pereira Nunes, J. P., Blunt, M. J., 2014. Statistical scaling of pore-scale Lagrangian velocities in natural porous media. Phys. Rev. E. 90, 023013, doi: 10.1103/PhysRevE.90.023013.

Silliman, S. E., Wright, A. L., 1988. Stochastic analysis of paths of high hydraulic conductivity in porous media. Water Resour. Res. 24(11), 1901-1910.

Siirila, E. R., Maxwell, R. M., 2012. Evaluating effective reaction rates of kinetically driven solutes in large-scale, statistically anisotropic media: Human health risk implications. Water Resour. Res. 48(4).

Strebelle, S., 2002. Conditional simulation of complex geological structures using multiple-point statistics. Math. Geol. 34(1), 1-21.

US EPA 2009, National Primary Drinking Water Regulations, EPA 816-F-09-004, May 2009.

van Leeuwen, M., Butler, A., te Stroet, C., Tompkins, J., 2000. Stochastic determination of well capture zones conditioned on regular grids of transmissivity measurements. Water Resour. Res. 36 (4), 949–957.

Vassolo, S., Kinzelbach, W., Schäfer, W., 1998. Determination of a well head protection zone by stochastic inverse modelling. J. Hydrol. 206 (3), 268–280.

Varljen, M. D., Shafer, J. M., 1991. Assessment of uncertainty in time-related capture zones using conditional simulation of hydraulic conductivity. Ground Water 29 (5), 737-748.

Vesselinov, V. V., 2007. Uncertainties in transient capture-zone estimates of groundwater supply wells. J. Contemp. Water Res. Educ. 137 (1), 1-7.

Wen, X.-H., Gómez-Hernández, J. J., 1998. Numerical modeling of macrodispersion in heterogeneous media: A comparison of multi-Gaussian and non-multi-Gaussian models. J. Contam. Hydrol. 30(1), 129-156, doi: 10.1016/S0169-7722(97)00035-1.

Willmann, M., Carrera, J., Sánchez-Vila, X., 2008. Transport upscaling in heterogeneous aquifers: What physical parameters control memory functions? Water Resour. Res. 44(12).

Xu, T., Gómez-Hernández, J. J., 2015. Inverse sequential simulation: A new approach for the characterization of hydraulic conductivities demonstrated on a non-Gaussian field. Water Resour. Res. 51, 2227-2242, doi:10.1002/2014WR016320.

Zheng, C., Wang, P. P., 1999. MT3DMS: A Modular Three-Dimensional Multispecies Transport Model for Simulation of Advection, Dispersion, and Chemical Reactions of Contaminants in Groundwater Systems; Documentation and User's Guide. Alabama Univ University.

Tables

Symbol	Significance	Units	Values
L_{sx}, L_{sy}	Aquifer Size	m	170, 150
$\Delta x, \Delta y$	Grid size	m	1/8 I, 1/8 I
J	Mean head gradient	-	0.59%
φ	Porosity	-	0.2
α_x	Longitudinal dispersivity	m	0.01
α_y	Transversal dispersivity	m	0.0001
x_w, y_w	Location of pumping well	m	114.5, 74.5
Q_w	Constant well pumping rate	m^3/d	0.3
Q_w	Variable well pumping rate	m^3/d	0.8/0/0.4/0/0.8/0/0.4/0/0.8/0/0.4/0/0.8/0/0.4/0
V_w	Volume of pumped water	m^3	1440
C^*	Concentration threshold	g/m^3	10
P_e	Péclet number	-	800

Table 1. Main parameters employed in the study.

Symbol	Significance	Units	Values			
			$\boldsymbol{\alpha = 1.2}$	$\boldsymbol{\alpha = 1.5}$	$\boldsymbol{\alpha = 1.8}$	$\boldsymbol{\alpha \to 2}$
I	Integral scale of Y	m	8.00	8.00	8.00	8.00
σ_Y^2	Variance of Y	-	3.00	3.00	3.00	3.00
$\mathcal{A}$	Constant	-	5.87×10^{-2}	17.53×10^{-2}	31.85×10^{-2}	35.75×10^{-2}
H	Hurst coefficient	-	0.33	0.33	0.33	0.33
λ_u	Upper cutoff scale	m	34.58	22.67	17.98	17.20
λ_l	Lower cutoff scale	m	1.00	1.00	1.00	1.00

Table 2. Parameters characterizing the transmissivity field.

Figures Captions

Fig. 1. Sketch of the problem analyzed.

Fig. 2. Pumping strategies (a) constant flow rate S_I and (b) variable flow rate S_{II}.

Fig. 3. Temporal evolution of the normalized mean concentration $\langle C \rangle$ observed at the pumping well for three values of $\alpha = 1.2, 1{,}5, 1.8$ and for a Gaussian Y field ($\alpha \to 2$). Results for pumping strategy (a) S_I and (b) S_{II}.

Fig. 4. Temporal evolution of the normalized concentration variance $Var[C]$ observed at the pumping well for three values of $\alpha = 1.2, 1{,}5, 1.8$ and for a Gaussian *Y* field ($\alpha \to 2$). Results for pumping strategy (a) S_I and (b) S_{II}.

Fig. 5. Pumping strategy S_I: Box plots of C_p for three values of $\alpha = 1.2, 1{,}5, 1.8$ and for a Gaussian *Y* field ($\alpha \to 2$).

Fig. 6. Pumping strategy S_{II}: Box plots of C_p for three values of $\alpha = 1.2, 1{,}5, 1.8$ and for a Gaussian *Y* field ($\alpha \to 2$).

Fig. 7. Pumping strategy S_I: Peak concentration PDF $p\left(C_p\right)$ for three values of $\alpha = 1.2, 1{,}5, 1.8$ and for a Gaussian *Y* field ($\alpha \to 2$). See inset for peak concentration CDF $P\left(C_p\right)$.

Fig. 8. Pumping strategy S_{II}: Peak concentration PDF $p(C_p)$ for three values of $\alpha = 1.2, 1,5, 1.8$ and for a Gaussian Y field ($\alpha \to 2$). See inset for peak concentration CDF $P(C_p)$.

Fig. 9. Relative impact of non-Gaussianity on the mean peak concentration C_p measured through η, see equation (6), for three values of $\alpha = 1.2, 1,5, 1.8$ and pumping strategy S_I (light grey) and S_{II} (dark grey).

Figures

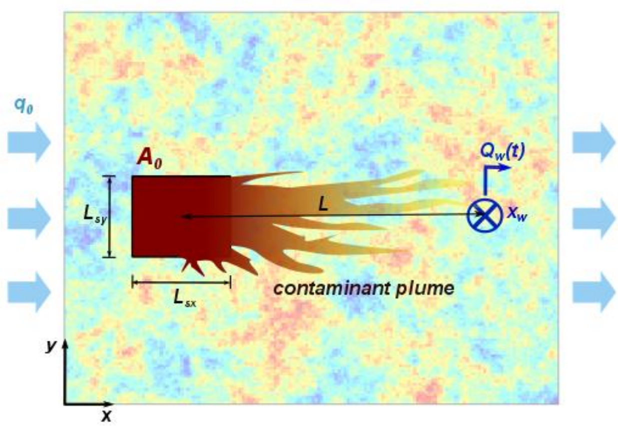

Fig. 1. Sketch of the problem analyzed.

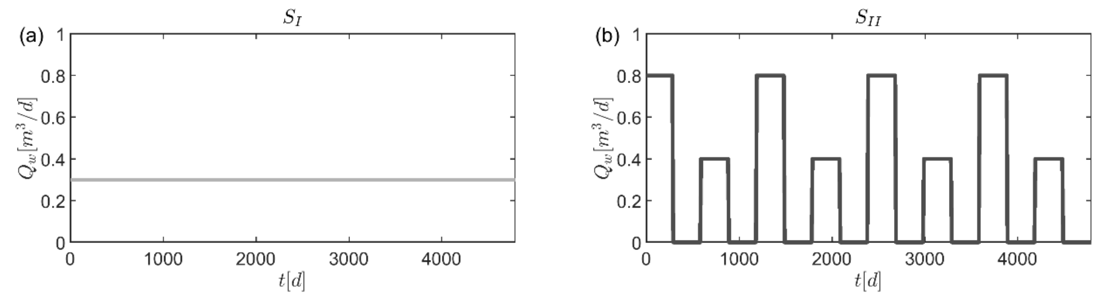

Fig. 2. Pumping strategies (a) constant flow rate S_I and (b) variable flow rate S_{II}.

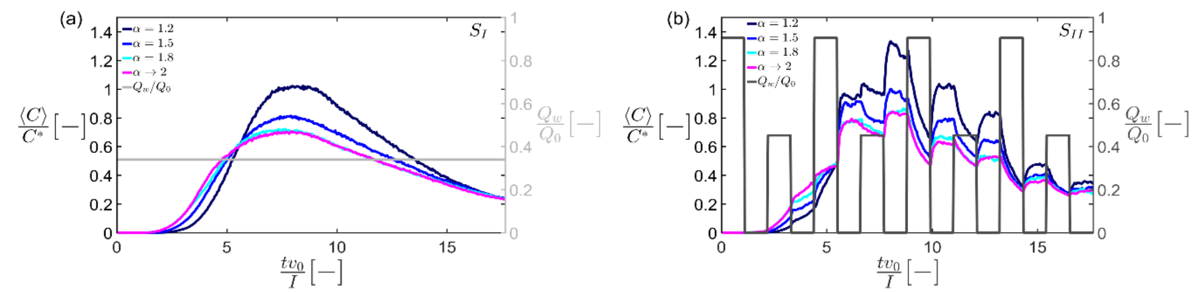

Fig. 3. Temporal evolution of the normalized mean concentration $\langle C \rangle$ observed at the pumping well for three values of $\alpha = 1.2, 1{,}5, 1.8$ and for a Gaussian Y field ($\alpha \to 2$). Results for pumping strategy (a) S_I and (b) S_{II}.

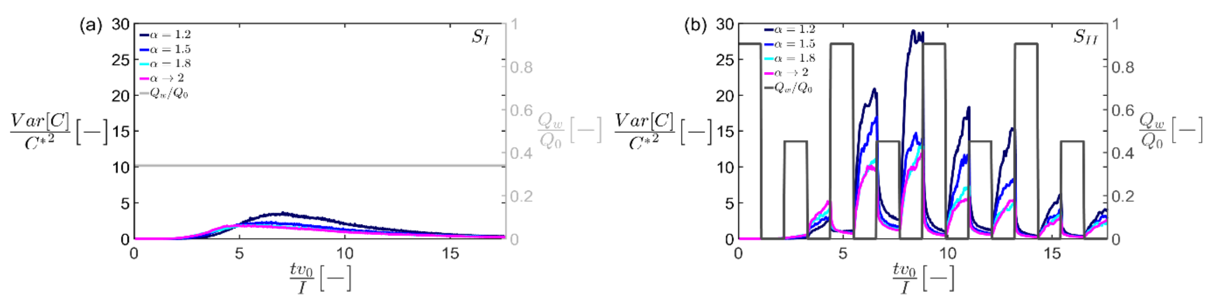

Fig. 4. Temporal evolution of the normalized concentration variance $Var[C]$ observed at the pumping well for three values of $\alpha = 1.2, 1{,}5, 1.8$ and for a Gaussian Y field ($\alpha \to 2$). Results for pumping strategy (a) S_I and (b) S_{II}.

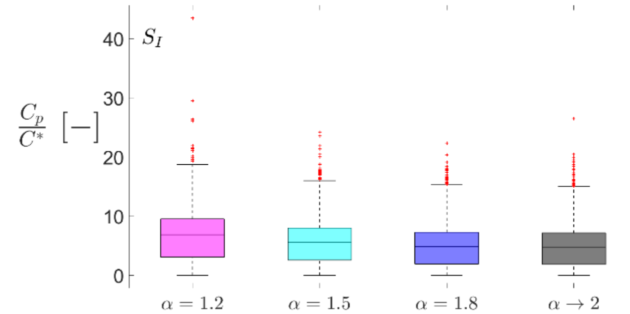

Fig. 5. Pumping strategy S_I: Box plots of C_p for three values of $\alpha = 1.2, 1{,}5, 1.8$ and for a Gaussian Y field ($\alpha \to 2$).

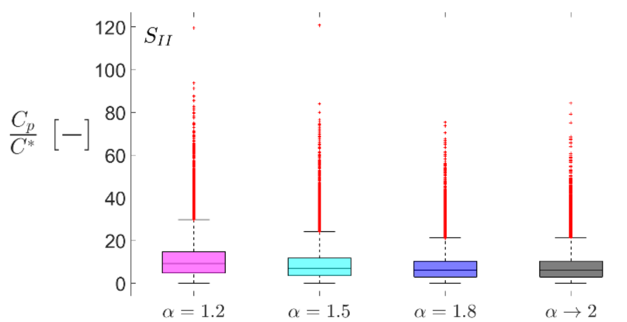

Fig. 6. Pumping strategy S_{II}: Box plots of C_p for three values of $\alpha = 1.2, 1{,}5, 1.8$ and for a Gaussian Y field ($\alpha \to 2$).

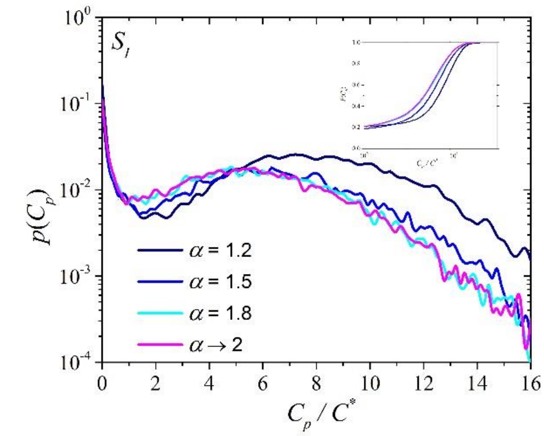

Fig. 7. Pumping strategy S_I: Peak concentration PDF $p(C_p)$ for three values of $\alpha = 1.2, 1{,}5, 1.8$ and for a Gaussian Y field ($\alpha \to 2$). See inset for peak concentration CDF $P(C_p)$.

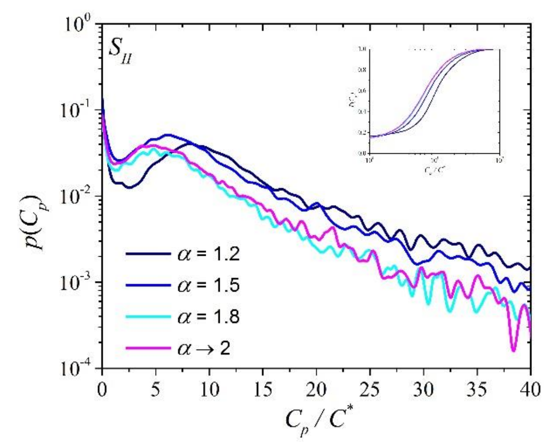

Fig. 8. Pumping strategy S_{II}: Peak concentration PDF $p(C_p)$ for three values of $\alpha = 1.2, 1{,}5, 1.8$ and for a Gaussian Y field ($\alpha \to 2$). See inset for peak concentration CDF $P(C_p)$.

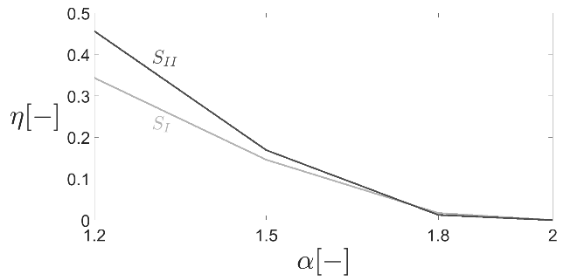

Fig. 9. Relative impact of non-Gaussianity on the mean peak concentration C_p measured through η, see equation (6), for three values of $\alpha = 1.2, 1{,}5, 1.8$ and pumping strategy S_I (light grey) and S_{II} (dark grey).